minerals

MDPI

Article

Amphibole Group Minerals in the Ozren Massif Ophiolites of Bosnia and Herzegovina as Petrogenetic Indicators

Samir Ustalić [1], Ondrej Nemec [1], Stanislava Milovská [2], Marián Putiš [1,*], Elvir Babajić [3], Sergii Kurylo [2] and Peter Ružička [1]

[1] Department of Mineralogy, Petrology and Economic Geology, Faculty of Natural Sciences, Comenius University, Ilkovičova 6, 842 15 Bratislava, Slovakia; ustalic1@uniba.sk (S.U.); ondrej.nemec@uniba.sk (O.N.); peter.ruzicka@uniba.sk (P.R.)
[2] Earth Science Institute of the Slovak Academy of Sciences, Ďumbierska 1, 974 11 Banská Bystrica, Slovakia; milovska@savbb.sk (S.M.); kurylo@savbb.sk (S.K.)
[3] Department of Mineralogy and Petrology, Faculty of Mining, Geology and Civil Engineering, University of Tuzla, Urfeta Vejzagića 2, 75 000 Tuzla, Bosnia and Herzegovina; elvir.babajic@untz.ba
* Correspondence: marian.putis@uniba.sk

Abstract: The Ozren ophiolite complex (OOC) of the Dinaridic Ophiolite Belt is one of the six ophiolite complexes in Bosnia and Herzegovina. This paper deals with the mineral chemistry of amphiboles determined by electron probe micro-analysis and micro-Raman spectroscopy. The detected amphibole generations and types in mafic, ultramafic, and metamorphic rocks suggest a polystage evolution and are therefore useful petrogenetic indicators of the investigated OOC. Most gabbroic rocks and dolerites contain primary magmatic amphibole1 (magnesio-hornblende to pargasite, occasionally hastingsite) and prismatic to needle-like aggregates of late magmatic amphibole2 (magnesio-hornblende), while plagiogranite contains ferri-winchite and ferro-ferri-winchite as primary magmatic amphibole. Post-magmatic amphiboles were detected in dolerites, troctolites, and lesser in peridotites. The Na-(Ti)-rich amphibole3 (ferri-winchite and ferro-ferri-winchite to katophorite and ferri-katophorite) with amphibole4 (grunerite) rim formed along the grain boundaries of clinopyroxene, amphibole1, and plagioclase in dolerites. A part of these amphiboles grows into amphibole1, 2. Kaersutite to ferri-kaersutite, associated with phlogopite, occur in troctolites and dunites, while Mhbl was detected in harzburgite. The ultramafic rocks (lherzolites, harzburgites, and dunites) and the gabbroic layer are crosscut by clinopyroxene–plagioclase gabbroic and clinopyroxene–plagioclase–amphibole gabbro–dolerite dykes, suggesting 'dry' and 'hydrated' percolating melts generated in inferred subridge and supra-subduction settings, respectively. The amphibole3 and 4 in gabbros and dolerites and similar amphibole types in ultramafic rocks could be related to inferred arc-type basaltic and plagiogranitic percolating melts and fluids. Low-Al amphibole5 (tremolite and actinolite) and associated chlorite, albite, and clinozoisite represent the ocean-floor alterations in mafic rocks. Amphibole6 (magnesio-hornblende to pargasite) was identified in metamorphic sole amphibolites. Micro-Raman spectroscopy provided typical Raman spectra for the studied amphiboles, highlighting distinct features such as bands related to ^{C}Mg content, $^{C}Fe^{3+}$ presence, TO_4 ring-breathing mode, TiO_6 stretching mode, presence >0.3 *apfu* of ^{C}Ti, and TO_4 stretching indicating $^{C}Fe^{2+}$ in the structure. Applied amphibole geothermobarometry revealed the formation P–T conditions of amphibole (Amp)1 (avg. 863 °C at 0.23 GPa), Amp2 (avg. 747 °C at 0.17 GPa), Amp in the mantle rocks (avg. 853 °C at 0.64 GPa), Amp5 (avg. 349 °C at 0.03 GPa), and Amp6 (avg. 694 °C at 0.46 GPa).

Keywords: amphiboles; mineral chemistry; micro-Raman spectroscopy; amphibole geothermobarometry; Ozren ophiolites; Bosnia and Herzegovina

check for updates

Citation: Ustalić, S.; Nemec, O.; Milovská, S.; Putiš, M.; Babajić, E.; Kurylo, S.; Ružička, P. Amphibole Group Minerals in the Ozren Massif Ophiolites of Bosnia and Herzegovina as Petrogenetic Indicators. *Minerals* **2024**, *14*, 239. https://doi.org/10.3390/min14030239

Academic Editors: Jingsui Yang, Souvik Das and Weiwei Wu

Received: 1 February 2024
Revised: 24 February 2024
Accepted: 24 February 2024
Published: 26 February 2024

Copyright: © 2024 by the authors. Licensee MDPI, Basel, Switzerland. This article is an open access article distributed under the terms and conditions of the Creative Commons Attribution (CC BY) license (https://creativecommons.org/licenses/by/4.0/).

1. Introduction

The amphibole group of minerals represents one of the most compositionally diverse mineral groups, and this diversity is reflected in the very different rock types, tectonic

environments, and wide range of P–T conditions in which they occur [1]. In general, magmatic amphiboles are very rare in ultramafic rocks, but they are mostly related to the gabbroic layers and dykes in ultramafic rocks and upper sequences of the ophiolite cross-sections (e.g., [2,3]). The presence of amphiboles and orthopyroxene with partly dissolved olivine in ultramafic rocks, may indicate a deep melt fractionation in magmatic arcs [4]. The arc magmas are commonly hydrated and crystallizing amphibole. Hornblende peridotites may indicate a reaction between a dunitic cumulate and an evolved hydrous melt around the Moho beneath the arcs [5,6]. Amphibole-rich mafic and ultramafic intrusive rocks could be a 'hidden' amphibole reservoir in the arc crust, and therefore amphibole plays a major role in the petrogenesis and differentiation of many arc magmas [7].

The Ozren ophiolite complex (OOC) is one of the six known ophiolite complexes in Bosnia and Herzegovina and the second largest (Figure 1; [8]). In this paper, we focused on the determination of representative amphiboles in plagiogranite (P5B), gabbro (P13B1), dolerite (P17C), troctolite (P18A), harzburgite (P21), and amphibolite (P10F), including the definition of amphibole chemistry by using electron probe micro-analysis (EPMA), as well as a description of the measured spectra and bands by using micro-Raman spectroscopy. We also determined uncommon Na–Ti amphibole phases such as ferro-ferri-katophorite reported by [9] as a new clinoamphibole from the silicocarbonatite dykes in Sierra de Maz, La Rioja, in Argentina.

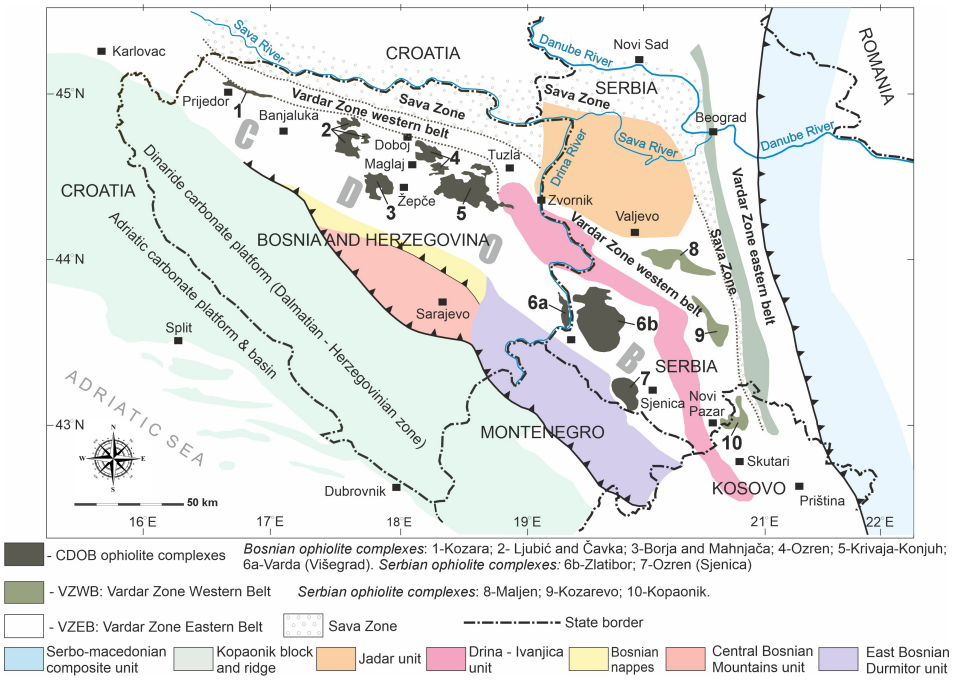


Figure 1. Ozren Massif (4) in Central Dinaridic Ophiolite Belt ([8]; map modified after [10,11]).

The main goal is to recognize and differentiate between all the amphibole types and decipher their relationship to the petrogenesis of the investigated OOC. The obtained dataset reveals less common (Na–Ti-rich) amphibole types, which are inferred to have originated due to basaltic and/or plagiogranitic percolating melts and fluids through peridotite and gabbro layers. Such amphibole-bearing rocks might have formed under the influence of arc-type magmas. We tried to use the determined amphibole generations for a petrogenetic interpretation, documenting their relationship to magmatic, post-magmatic melt/fluid-rock interaction, and the metamorphic evolutional stages of the OOC. We estimated the formation P–T conditions of amphiboles using the chosen amphibole geothermobarometers.

2. Geological Setting

The Dinaride ophiolite belt represents one of the most remarkable stratigraphic units along the entire Balkan, which is a branch of the Alpine–Himalayan Tethyan orogenic belt. The Dinaridic segment of Neotethys was affected by widespread shortening and related subduction–obduction–accretion processes that commenced in the Middle Jurassic. The Dinaride ophiolites belong either to the Central Dinaridic Ophiolite Belt (CDOB) or to the Vardar zone (VZ, also called IDOB = Inner Dinaridic Ophiolite Belt). While areas of the VZ ophiolites are of supra-subduction origin, the dismembered CDOB ophiolites are associated with the ocean-ridge geotectonic environment. The CDOB and VZ Western Belt are collectively referred to as the Western Vardar Ophiolite Unit to distinguish them from the ophiolites of the Eastern Vardar Ophiolite Unit (or Main Vardar Belt), separated from the Western Unit by the Sava Zone (Figure 1).

The Ozren ophiolite complex (OOC) in Bosnia and Herzegovina is part of the Dinaridic Ophiolite Belt [8,10–23]. This complex shows a polystage mantle evolution and revealed an almost complete ophiolitic cross-section composed of peridotites, plagioclase peridotites, plagiogranites, troctolites, and other gabbros, gabbroic, doleritic, and fewer basaltic dykes. Pillow basalts are alternating or covered by Bajocian to Bathonian radiolarites [24,25]. Metamorphic sole amphibolites may indicate intraoceanic subduction. A sheeted dyke layer is missing in this ophiolitic complex (Figure 2a,b).

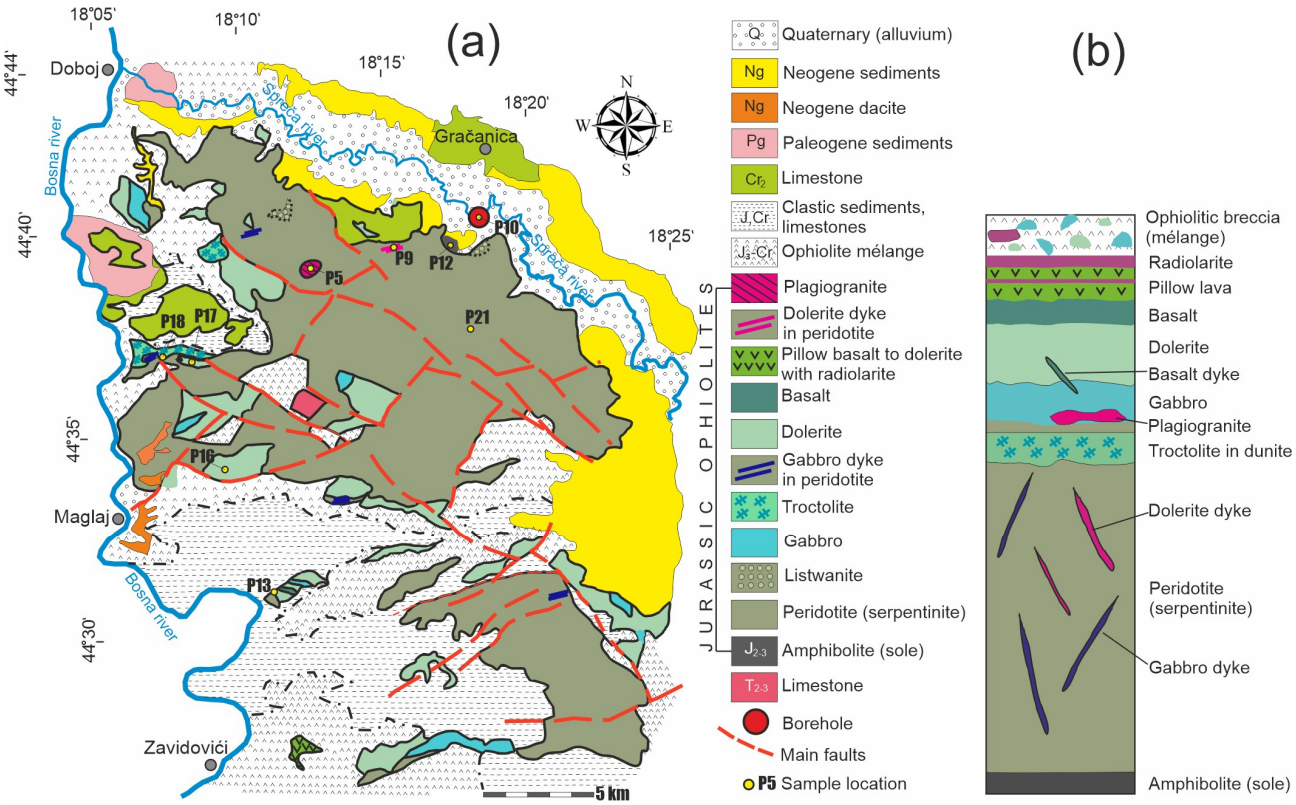


Figure 2. Ozren ophiolite complex and mélange. (**a**) geological map compiled from the basic geological map of the former SFR Yugoslavia 1:100,000, and new data from the investigation with sample numbers (map modified after [8,25–27]; (**b**) a schematic cross-section (not to scale).

3. Materials and Methods

The fieldwork was focused on finding relatively fresh rocks that contain amphiboles suitable for further laboratory analyses (Figure 2a; see GPS of the sample location in Table 1). All principal rock types were first studied in transmitted light from the polished rock sections by a polarized light microscope. Representative samples were used for further investigation by electron probe micro-analysis (EPMA) and micro-Raman spectroscopy.

Table 1. GPS coordinates of investigated samples with amphiboles in Figure 2.

Samples	GPS Coordinates
P5B Plagiogranite	N 44°39′1.80″, E 18°12′25.32″
P9 Dolerite	N 44°39′43.82″, E 18°15′7.98″
P10A Gabbro	N 44°40′36.61″, E 18°17′40.59″
P10C Gabbro	N 44°40′36.61″, E 18°17′40.59″
P10D Basalt	N 44°40′36.61″, E 18°17′40.59″
P10F Amphibolite	N 44°40′36.61″, E 18°17′40.59″
P12A Amphibolite	N 44°39′44.33″, E 18°17′25.70″
P13B1 Gabbro	N 44°30′40.86″, E 18°11′29.58″
P13B2 Leucogabbro	N 44°30′40.86″, E 18°11′29.58″
P16 Dolerite	N 44°34′15.72″, E 18°9′18.84″
P17B, C Dolerite	N 44°37′8.26″, E 18°8′11.46″
P18A Troctolite	N 44°36′52.06″, E 18°7′4.42″
P18D Dunite	N 44°36′52.06″, E 18°7′4.42″
P21 Harzburgite	N 44°37′42.00″, E 18°13′58.86″

The chemical compositions of amphiboles were acquired using wavelength-dispersive (WDS) analyses on a CAMECA SX-100 electron probe microanalyzer at the State Geological Institute of Dionýz Štúr in Bratislava, and by the JEOL Super-probe JXA-8530F at the Earth Science Institute of Slovak Academy of Sciences in Banská Bystrica, Slovakia. The electron beam accelerating potential was 15 kV, with a beam current of 20 nA and a beam diameter of 3–5 μm. Measured lines, crystals, and spectrometers were Si (TAP, Kα, and wollastonite), F (LPCO, Kα, and LiF), Cl (LPET, Kα, and NaCl), Al (TAP, Kα, and Al_2O_3), Ca (LPET, Kα, and apatite), Fe (LLIF, Kα, and fayalite), Ti (LLIF, Kα, and TiO_2), K (LPET, Kα, and orthoclase), Na (TAP, Kα, and albite), Mg (TAP, Kα, and forsterite), Mn (LLIF, Kα, and rhodonite), Cr (LLIF, Kα, and Cr), Ni (LLIF, Kα, and Ni), V (LLIF, Kα, and V), and Zn (LLIF, Kα, and willemite).

Raman spectroscopic measurements of thin sections were performed on a Labram HR800 microspectrometer (Horiba Jobin-Yvon), connected to an Olympus BX41 microscope with confocally coupled Czerny–Turner-type monochromator (focal length 800 mm) at the Earth Science Institute of the Slovak Academy of Sciences in Banská Bystrica, Slovakia. A frequency-doubled Nd-YAG laser at 532 nm was used for excitation (633 nm for verifying/excluding of luminescence effect). The Raman-scattered light was collected in 180° geometry through a 50× and 100× objective lens with numerical aperture 0.8 (100×) and dispersed by diffraction grating with 600 grooves per mm. System uses CCD detector (cooled charge-coupled device). The system resolution was 6 cm^{-1}. The grating turret accuracy was calibrated between the zero-order line (180° reflection) and the laser line at 0 cm^{-1}. Spectral accuracy was verified on the 734 cm^{-1} band of Teflon.

All determined amphiboles from this ophiolite complex are classified based on mineral calculation [28] and suitable diagrams [29,30].

Methodical Approach for the Calculation of Amphiboles

- All amphiboles are calculated with [28] Excel Spreadsheet;
- Calculations are based on 15 cations following one of 2 procedures: (1) Si to Ca&Li = 15 *apfu* for Ca amphiboles (Mhbl, Prg, and Hst) and (2) Si to Na = 15 *apfu* for Gru, Krs, and Wnc;
- Fe^{3+} was calculated based on charge balance;
- OH was calculated based on assumption 2 (OH, F, and Cl);
- For Ti-rich samples, estimation of OH content was set according to OH = 2-2^{C}Ti. This estimate provides minimum OH; structure refinement provides more accurate results: [31] recommended for $^{C}Ti \geq 0.1$; roughly >1.0 wt.% TiO_2 by [28];
- Mineral formula assigned based on 24 anions.

Amphibole geothermobarometry was used to constrain the P–T conditions of investigated samples. We used a combination of single-Amp geothermobarometry by [32] and Al and Ti-in-Amp geothermobarometry by [33].

Abbreviations of the rock-forming mineral names used in the text, tables, and figures are from [34] or adapted for this paper (marked by *): Ab, albite; Act, actinolite; Amp, amphibole; Bt, biotite; Chl, chlorite; Cpx, clinopyroxene; Czo, clinozoisite; Ep, epidote; Fkrs, ferri-kaersutite; Fktp, ferri-katophorite; Fwnc, ferri-winchite; Fe-Wnc*, ferro-ferri-winchite; Gru, grunerite; Hst, hastingsite; Ilm, ilmenite; Krs, kaersutite; Ktp, katophorite, Mhbl, magnesio-hornblende; Ol, olivine; Opx, orthopyroxene; Phg*, phengite; Phl, phlogopite; Pl, plagioclase; Prg, pargasite; Sdg, sadanagaite; Qz, quartz; Spl, spinel; Str, strontianite; Ti-Sdg*, Ti-rich sadanagaite; Tr, tremolite; Ttn, titanite; and Zo, zoisite.

4. Results

4.1. Petrographic Description of Samples

Petrographic description of samples was completed from polished rock thin sections, which were used for further analytical investigations by EPMA and micro-Raman techniques.

Gabbro (sample P10C; Figures 2 and 3a) contains coarse-grained Cpx, Pl, and Amp. Prismatic to needle-like Amp aggregates occur in grain boundaries of coarse-grained Amp, Cpx, and Pl and on the rim of this Amp. A gradual transition between these two Amp types is often observable. Pyroxene and Amp margins are partly replaced by micro-needle Amp and Chl aggregates. Plagioclase is weakly altered.

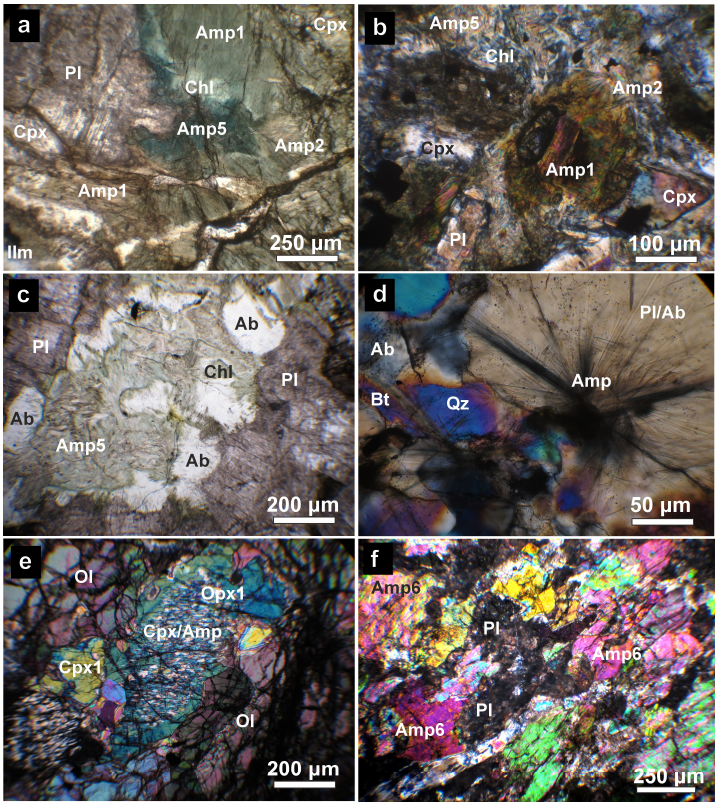


Figure 3. PL microscopic images of Amp: (**a**) Cpx-Pl-Amp-Ilm gabbro (P10C) with blue–green rim of Amp-Chl aggregates; (**b**,**c**) Cpx-Pl-Amp dolerite (P17C) with secondary aggregates of Chl, Amp, Czo, and Ab; (**d**) plagiogranite (P5B) texture composed of Qz, Pl/Ab, Bt, and needle-like Amp; (**e**) harzburgite (P21) contains Opx1 and Cpx1 porphyroclasts with exsolution lamellae accompanied by Amp; (**f**) sole amphibolite (P12A) texture with Amp-Pl preferred orientation. Pictures (**a**,**c**) at *II* P; (**b**,**d**–**f**) at *X* P.

Dolerite (sample P17C; Figures 2 and 3b,c) shows a magmatic texture defined by porphyritic Cpx, Amp, and Pl, with an accessory opaque phase. This dolerite also contains needle-like aggregates in grain boundaries of Cpx, porphyritic Amp, and Pl, as well as on the rims of the porphyritic Amp. Transitions from Amp1 to Amp2 are visible in a microscope. Other hypidiomorphic to idiomorphic tiny individual Amp grains are observable, and all the mentioned Amp habits and Px are enclosed in very fine-grained and micro-needle-like Amp aggregates in association with Chl, Czo, and Ab.

A plagiogranite body (sample P5B; Figures 2 and 3d) occurs in direct contact with peridotite (Figure 2). It is composed of Pl, Qz, Bt, needle-like Amp aggregates, and an opaque phase. Biotite is partly replaced by Chl and Ttn.

Harzburgite (sample P21; Figures 2 and 3e) contains Opx1 porphyroclasts with inferred Cpx exsolution lamellae.

Troctolite (sample P18A; Figure 2) exclusively occurs within the dunite layers in peridotites. The Ol–Spl matrix is enriched in Pl and less in Cpx. The contact between Ol and Pl is accompanied by interstitial Cpx enclosing Ol and/or Spl. Olivine is serpentinized, while Pl underwent albitization and additional alterations.

The sole Pl amphibolites (sample P12A; Figures 2 and 3f) contain parallel-oriented Amp porphyroblasts, which are dynamically recrystallized into fine-grained Amp aggregates. Both Amp generations are partly replaced by Chl, needle-like Amp, and Czo, while Pl is albitized.

4.2. Chemical Composition of Amphiboles

Using EPMA, a few Amp types with varying chemical compositions were identified in the rock textures (Figure 4a–h). The determined amphiboles belong to a wide range of Amp subgroups ranging from calcic and sodic–calcic to magnesium–iron–manganese subgroup and oxo-amphiboles according to the classification of [30] (Figure 5a–c) and the classification of [29] (Figure 5d). Tables 2 and S1 display the mineral chemistry variations in the amphiboles of the OOC. Table 3 provides the genetic criteria for the Amp types. Table S1 contains recalculated amphibole analyses, which we also used in the geothermobarometry (Section 4.4).

Table 2. Mineral chemistry of amphiboles in the Ozren ophiolite complex from [8]. Amphibole 1 to 5 types were determined in the gabbro layer mafic rocks (gabbros and dolerites) and basalts, while Amp6 from the sole amphibolites. The other Amp types were detected in plagiogranite and ultramafic rocks (harzburgite, dunite, and troctolite).

Oxide (wt.%).	SiO_2	TiO_2	Al_2O_3	Cr_2O_3	FeO	MgO	CaO	Na_2O
Harzburgite—P21								
Amp-P21 (following Cpx exsol. lamellae in Opx)	48.08–48.86	0.24–0.34	10.90–11.84	1.19–2.22	2.46–2.84	18.51–18.92	11.95–12.47	0.91–1.10
Dunite—P18D								
Amp-P18D (from percolating melt/fluids, incl. Phl)	42.23–43.96	3.28–4.83	11.10–12.26	2.32–2.97	3.61–4.06	16.40–17.44	10.43–11.68	4.20–4.91
Troctolite—P18A								
Amp-P18A (from percolating melt/fluids, incl. Phl)	40.55–46.03	3.48–5.47	11.09–16.94	1.39–3.39	1.52–2.92	16.77–25.68	0.11–11.65	0.75–6.29
Gabbro—P10A-C,13B1,13B2								
Amp1 (magmatic)	43.04–51.11	0.10–3.50	5.31–10.03	0.00–0.04	10.53–22.29	9.20–16.96	0.05–11.80	0.74–2.44
Amp2 (late magmatic)	44.91–51.77	0.07–3.07	5.02–11.60	0.00–0.33	8.52–17.86	10.33–17.11	9.67–11.66	0.16–2.58
Amp5 (post-magmatic alteration)	51.44–55.87	0.11–0.32	1.91–3.35	0.00–0.16	8.28–19.66	11.23–19.50	10.53–12.97	0.23–0.46
Plagiogranite—P5B								
Amp1 (magmatic)	53.11–57.03	0.30–1.63	0.08–0.19	0.00–0.03	15.13–25.69	6.59–13.57	4.50–6.66	3.70–5.95

Table 2. *Cont.*

Oxide (wt.%).	SiO_2	TiO_2	Al_2O_3	Cr_2O_3	FeO	MgO	CaO	Na_2O
Dolerite—P9,16,17C								
Amp1 (magmatic)	41.62–52.24	0.10–3.85	4.45–12.86	0.00–0.43	10.74–17.07	12.20–15.37	8.87–11.72	0.47–3.33
Amp2 (late magmatic)	45.25–53.88	0.09–1.12	4.86–11.62	0.00–0.07	11.02–17.70	11.00–17.20	9.65–11.34	0.38–2.24
Amp3-P17C (from percolating melt/fluids)	50.86–53.22	1.33–4.13	0.83–15.05	0.00	17.90–27.24	6.08–12.44	4.26–9.49	2.98–4.90
Amp4-P17C (from percolating melt/fluids)	51.67–53.68	0.17–1.14	0.25–1.03	0.00–0.02	28.02–33.94	8.15–12.32	0.83–4.97	0.24–0.73
Amp5 (post-magmatic alteration)	51.67–58.93	0.03–1.56	0.42–3.66	0.00–0.06	4.94–28.04	6.49–20.94	4.67–12.66	0.03–1.02
Basalt—P10D								
Amp1-P10D (magmatic)	40.18–50.46	0.11–2.73	4.84–14.94	0.00–0.09	13.05–16.75	9.51–15.83	11.42–12.23	1.00–2.71

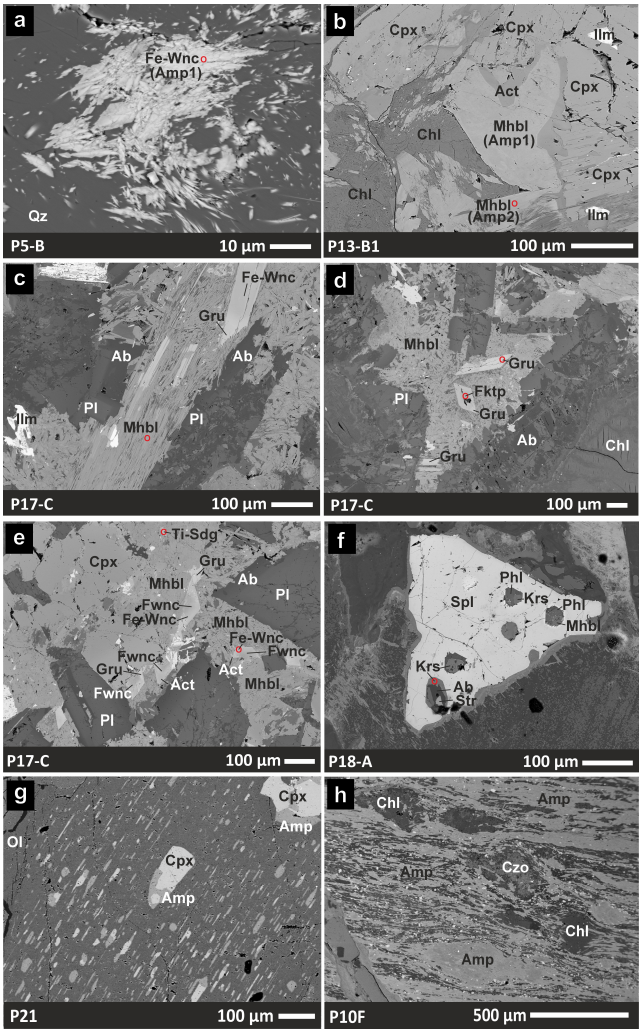


Figure 4. Backscattered electron images of analyzed samples from gabbro layer (**a**–**e**), troctolite (**f**), harzburgite (**g**), and amphibolite (**h**): (**a**) plagiogranite (P5B) with needle-like Amp1 (Fe-Wnc) aggregates in Qz; (**b**) Cpx-Pl-Amp-Ilm gabbro (P13B1) with magmatic Amp1,2 (Mhbl) and newly formed aggregates of Amp5 (Tr and Act) and Chl; (**c**–**e**) Cpx-Pl-Amp-Ilm dolerite (P17C) with the primary magmatic Amp1, late magmatic Amp2, and the post-magmatic Amp3–5 types; (**f**) troctolite (P18A) shows partial replacement of Spl by Amp (Mhbl and Krs), Phl, Ab, and Str in Ab; (**g**) harzburgite (P21) Opx with Cpx and Amp-Mhbl exsolution lamellae; (**h**) amphibolite (P10F) with Amp (Mhbl and Prg) porphyroclasts (porphyroblasts originally) in sheared matrix of dynamically recrystallized Mhbl and Prg, partly replaced by Tr, Act, Ep, Czo, Phg, Ab, and Chl. The red circles are the places where the samples were analyzed by both EPMA and micro-Raman spectroscopy.

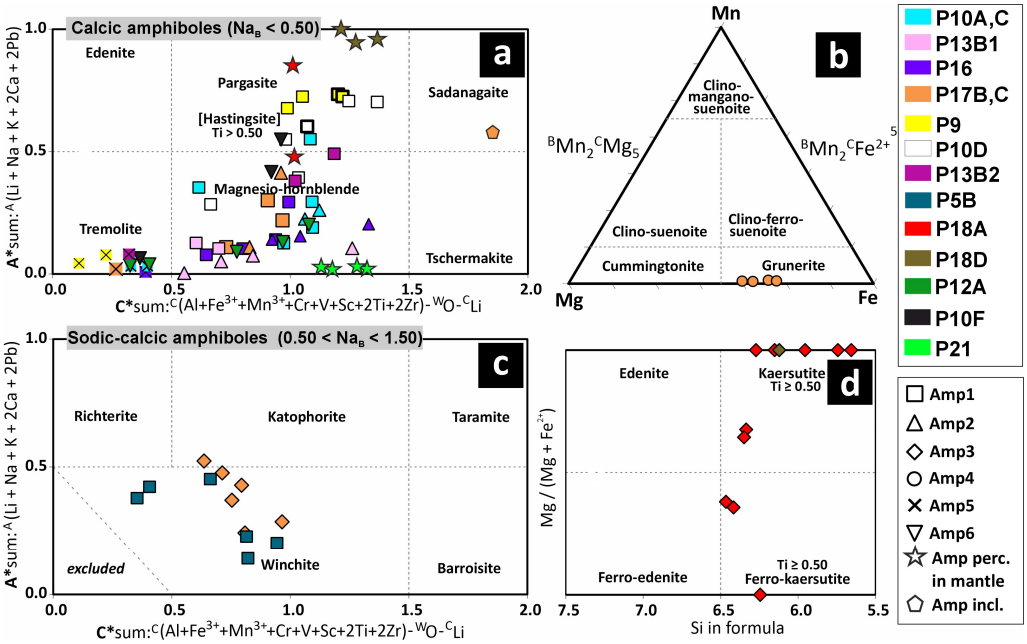


Figure 5. Amphibole chemistry in rocks from the Ozren ophiolite complex: (**a**–**c**) classification of [30]; (**d**) classification of [29]. Amphibole1 with thick frame in (**a**) is Hst. The rock types and their GPS coordinates are in Table 1.

Table 3. Review of Amp genetic types based on petrography and mineral chemistry criteria.

Amphibole Type	Genesis	Criterion 1	Criterion 2	Criterion 3
Amp1-Mhbl, Prg, Hst in gabbro, dolerite, basalt	Primary magmatic	Rock-forming	Coexisting with Cpx, Pl	Replaced by Amp5
Amp1-Wnc in plagiogranite	Primary magmatic	Rock forming	Coexisting with Pl, Qz	Rare
Amp2-Mhbl in gabbro, dolerite	Late magmatic	Following Amp1 rims	Chemistry like Amp1	Replaced by Amp5
Amp3-Wnc, Ktp in gabbro, dolerite	From percolating melts/fluids	Growing into Amp1, 2	Idiomorphic, hypidiomorphic	Rare, irregularly distributed
Amp4-Gru in gabbro, dolerite	From percolating melts/fluids	Enclosing Amp3	Outer zone on Am3	Rare, irregularly distributed
Amp5-Tr, Act in gabbro, dolerite, basalt	Post-magmatic alteration	Replacing Amp1–4	Associated with Chl, Ab, Czo	Common
Amp6-Mhbl, Prg in sole amphibolite	Metamorphic	Parallel-oriented aggregate	Associated with Pl	In sole amphibolite
Amp-Sdg inclusion in Amp1 in dolerite	Xenocryst? relict	Tiny inclusions in Amp1	Rare	
Amp-Hbl, Prg, Krs in troctolite	From percolating melts/fluids	Reaction zone with Spl	Associated with Phl, Pl and Cpx	Rare
Amp-Hbl in harzburgite	Exsolution system in Opx	Single Amp or common Cpx-Amp exsolution lamellae in Opx	Single Amp type in harzburgite	Rare

Plagiogranite (sample P5B) contains Fe-Wnc to Fwnc as the principal Amp types (Figures 4a and 5c), while the composition of Amp1 in gabbros, dolerites, and basalts corresponds to Mhbl and Prg, rarely to Hst (Figures 4b–e and 5a). The TiO_2 amphibole content in the gabbros, dolerites, and basalts is between 0.10 and 3.85 wt.%, while, in plagiogranites, it is commonly less, reaching up to 1.63 wt.%. The Al_2O_3 amphibole values are mostly lower in the gabbros, from 5.31 to 10.03 wt.%, and reach up to 14.94 wt.% in the basalts and dolerites. Very low values between 0.08 and 0.19 wt.% are found in the Amp of plagiogranite. The amphibole (Fe-Wnc to Fwnc) from plagiogranite (sample P5B) has the highest content of Na_2O (3.70–5.95 wt.%). In the gabbros, dolerites, and basalts, the Na_2O amphibole content is generally lower, between 0.47 and 3.33 wt.% (Tables 2 and S1).

In the gabbros and dolerites, Amp2 is represented by prismatic to needle-like Mhbl aggregates (Figures 4b–e and 5a). In the gabbros, the TiO_2 amphibole content ranges from 0.07 to 3.07 wt.%, whereas, in the dolerites, it is significantly lower, ranging from 0.09 to 1.12 wt.%. The Al_2O_3 amphibole values in the gabbros and dolerites are very similar

(4.86–11.62 wt.%). The same situation occurs with the Na_2O content in these rocks (0.16–2.58 wt.%) (Tables 2 and S1).

Dark (in BSE) Amp3, which is represented by Fe-Wnc, Fwnc, Ktp, and Fktp (Figures 4d–e and 5c), was found in the core of Amp4 grains in dolerite (sample P17C). A few individual tiny grains are Sdg to Ti-Sdg (Figures 4e and 5a) enclosed in Amp1. Pale Amp4 (Gru) is on the rim of the Amp3 grains (Figures 4d–e and 5b). Amphibole3 has higher content of TiO_2 between 1.33 and 4.13 wt.%. Amphibole4 reaches up to 1.14 wt.%. The Al_2O_3 content in Amp3 is 0.83–15.05 wt.% and 0.25–1.03 wt.% in Amp4. The determined Amp3 is particularly characterized by increased Na_2O content compared to the Amp4 generation (2.98–4.90 wt.% in Amp3; 0.24–0.73 wt.% in Amp4) (Tables 2,3 and S1). We also determined Krs to Fkrs, or Mhbl to Prg in association with Cpx and Phl in troctolite (Figure 4f) and dunite (samples P18A and P18D, respectively) (Figure 5a,d), while an Amp in harzburgite is Mhbl (Figure 4g).

The low-Al Amp5 is represented by Tr, Act aggregates that overgrow and partly to totally replace the Amp1–4 generations, and Cpx in mafic rocks (Figures 4b,e and 5a). The content of TiO_2 in Amp5 ranges from 0.03 to 1.56 wt.%. The content of Al_2O_3 and Na_2O is between 0.42 and 3.66 wt.% and 0.03–1.02 wt.%, respectively (Tables 2 and S1).

The amphibolites (samples P10F and P12A) contain metamorphic Amp6-Mhbl to Prg, and newly formed Tr and Act (Figure 5a). The mineral chemistry of the representative amphiboles is shown in Table 2 and Table S1.

4.3. Results of Micro-Raman Spectroscopy

At the same analytical spots where we analyzed the representative amphiboles by EPMA (Figure 4a–f; Table 4), we also examined in detail the Raman spectra of these amphiboles (Figure 6a–h). All the samples have a distinct band at around 150 cm^{-1} (Figure 6a–h), where the most distinctly visible band is on the Krs spectra (Figure 6h). The majority of the analyzed Raman spectra (Fe-Wnc, Fktp, Ti-Sdg, and Krs; Figure 6a,d,f–h) are characterized by enhanced Raman scattering near 530 cm^{-1} to 570 cm^{-1}, while this band is suppressed regarding Mhbl (Figure 6b) and Gru (Figure 6e) spectra. The strongest peak for all the amphibole spectra is at 670 cm^{-1} (Figure 6a–h). Ti-rich sadanagaite and Krs spectra (Figure 6f,h) reveals a peak at 750 cm^{-1} to 800 cm^{-1}, while this peak is not visible on any other spectra. All the Raman spectra, except the Krs spectra, contain a Raman peak at around 1040 cm^{-1} (Figure 6a–h). Raman vibrations of OH- stretching were visible in all the analyzed samples at 3640–3660 cm^{-1}.

Table 4. Table of representative microprobe analyses of amphiboles measured by both EPMA and micro-Raman spectroscopy. Amphibole types according to Tables 2,3 and S1.

Type of Amp	**Fe-Wnc**	**Mhbl**	**Mhbl**	**Fktp**	**Ti-Sdg**	**Fe-Wnc**	**Krs**	**Gru**
Sample/an	P5B/20	P13B1/22	P17C/1	P17C/19	P17C/25	P17C/36	P18A/6	P17C/21
Spectra	sp13-Amp1	sp7-Amp1	sp1-Amp2	sp16-Amp3	sp32-incl. in Amp1	sp41-Amp3	sp24-Amp	sp18-Am4
				Analysis (wt.%)				
SiO_2	53.42	51.50	50.06	53.16	39.00	52.91	43.21	52.73
TiO_2	0.41	0.17	0.53	1.55	4.13	1.38	5.17	0.17
Al_2O_3	0.08	5.02	5.55	1.18	15.05	0.83	13.81	0.25
V_2O_3	0.01	0.00	0.02	0.14	0.04	0.07	0.11	0.01
Cr_2O_3	0.01	0.00	0.00	0.00	0.00	0.00	2.11	0.02
MnO	0.13	0.05	0.44	0.27	0.39	0.25	0.00	0.59
FeO	25.69	16.79	17.70	17.90	19.98	24.08	2.69	33.94
NiO	0.00	0.00	0.07	0.00	0.02	0.00	0.06	0.02
ZnO	0.28	0.05	0.17	0.25	0.15	0.13	0.17	0.37
MgO	6.59	12.29	12.15	12.44	6.49	9.08	16.77	9.71
CaO	5.71	9.67	9.87	5.62	9.49	4.57	11.58	0.83
Na_2O	4.42	0.16	1.00	4.90	2.98	4.69	0.82	0.09
K_2O	0.94	0.01	0.04	0.46	0.05	0.57	0.27	0.00
F	0.57	0.03	0.06	1.13	0.13	0.49	0.00	0.80
Cl	0.00	0.01	0.07	0.02	0.03	0.06	0.01	0.04
Initial Total	**98.28**	**95.73**	**97.74**	**99.02**	**97.93**	**99.09**	**96.78**	**99.56**

Table 4. *Cont.*

Type of Amp	Fe-Wnc	Mhbl	Mhbl	Fktp	Ti-Sdg	Fe-Wnc	Krs	Gru
				Final wt.% values				
MnO	0.13	0.05	0.44	0.27	0.39	0.25	0.00	0.59
Mn_2O_3	0.00	0.00	0.00	0.00	0.00	0.00	0.00	0.00
FeO	23.35	16.79	15.16	15.61	17.88	20.80	0.00	33.94
Fe_2O_3	2.61	0.00	2.83	2.54	2.33	3.64	2.99	0.00
H_2O+	1.70	2.00	2.00	1.51	1.91	1.77	0.91	1.58
Total	**100.04**	**97.71**	**99.98**	**100.33**	**100.06**	**101.03**	**98.00**	**100.86**
				Formula Assignments (*apfu*)				
Si	8.122	7.638	7.339	7.794	5.912	7.871	6.239	8.039
Al	0.000	0.362	0.661	0.204	2.088	0.129	1.761	0.000
Ti	0.000	0.000	0.000	0.002	0.000	0.000	0.000	0.000
ΣT	**8.122**	**8.000**	**8.000**	**8.000**	**8.000**	**8.000**	**8.000**	**8.039**
Ti	0.047	0.018	0.059	0.169	0.471	0.155	0.562	0.019
Al	0.015	0.516	0.299	0.000	0.601	0.016	0.589	0.046
V	0.002	0.000	0.002	0.017	0.005	0.008	0.013	0.001
Cr	0.002	0.000	0.000	0.000	0.000	0.000	0.241	0.003
Fe^{3+}	0.298	0.000	0.312	0.281	0.266	0.407	0.325	0.000
Ni	0.000	0.000	0.008	0.000	0.003	0.003	0.007	0.003
Zn	0.032	0.005	0.018	0.027	0.017	0.014	0.019	0.041
Mn^{2+}	0.017	0.000	0.000	0.000	0.000	0.000	0.000	0.000
Fe^{2+}	2.969	1.744	1.646	1.785	2.164	2.383	0.000	2.672
Mg	1.492	2.717	2.656	2.719	1.467	2.013	3.244	2.207
ΣC	**4.874**	**5.000**	**5.000**	**4.998**	**4.994**	**4.999**	**5.000**	**4.992**
Mn^{2+}	0.000	0.007	0.054	0.033	0.050	0.032	0.000	0.076
Fe^{2+}	0.000	0.339	0.213	0.129	0.103	0.205	0.000	1.655
Mg	0.000	0.000	0.000	0.000	0.000	0.000	0.366	0.000
Ca	0.930	1.536	1.551	0.883	1.541	0.728	1.634	0.136
Na	1.070	0.045	0.182	0.955	0.306	1.035	0.000	0.025
ΣB	**2.000**	**1.927**	**2.000**	**2.000**	**2.000**	**2.000**	**2.000**	**1.892**
Ca	0.000	0.000	0.000	0.000	0.000	0.000	0.157	0.000
Na	0.233	0.000	0.103	0.437	0.570	0.316	0.230	0.000
K	0.182	0.001	0.008	0.086	0.009	0.107	0.050	0.000
ΣA	**0.415**	**0.001**	**0.111**	**0.523**	**0.579**	**0.423**	**0.437**	**0.000**
O (non-W)	22.000	22.000	22.000	22.000	22.000	22.000	22.000	22.000
OH	1.724	1.982	1.954	1.472	1.931	1.758	0.873	1.606
F	0.276	0.015	0.029	0.523	0.061	0.228	0.000	0.384
Cl	0.000	0.003	0.017	0.005	0.007	0.014	0.003	0.010
O	0.000	0.000	0.000	0.000	0.000	0.000	1.124	0.000
ΣW	**2.000**	**2.000**	**2.000**	**2.000**	**1.999**	**2.000**	**2.000**	**2.000**
Σ T, C, B, A	**15.416**	**14.928**	**15.111**	**15.524**	**15.578**	**15.422**	**15.438**	**14.931**

4.4. Amphibole Geothermobarometry Results

Amphibole geothermobarometry was used to constrain the P–T condition of the genetically different Amp groups and types reviewed in Tables 5 and S1. Among the Amp geothermobarometers, we used a combination of single-Amp geothermobarometry by [32] and Al and Ti-in-Amp geothermobarometry by [33]. Magmatic Amp1, 2 constrained the crystallization T of gabbros and dolerites during the formation of the gabbro–dolerite layer of the OOC. The group of Amp3, 4 was not suitable for any Amp geothermobarometric method because of these amphiboles' specific chemical composition that falls outside of their calibration constraints (Figure 5; Tables 2 and S1). Tiny inclusions of Sdg and Ti-Sdg within Amp1 (Figures 4e and 5), although suitable for geothermobarometric estimates, are most likely not primary magmatic phases of dolerite (P17C) in the gabbro–dolerite layer (also see Sections 5.1 and 5.3). On the other hand, part of the rare amphiboles (Amp percolation type in Figure 5 and Tables 2 and S1) from ultramafic rocks, such as harzburgites, dunites, and troctolites, provided P–T conditions regarding their formation. Similarly, the Amp5 from gabbros and dolerites provided reasonable results. Also, metamorphic Amp6 from the sole amphibolites was suitable for using the chosen geothermobarometers.

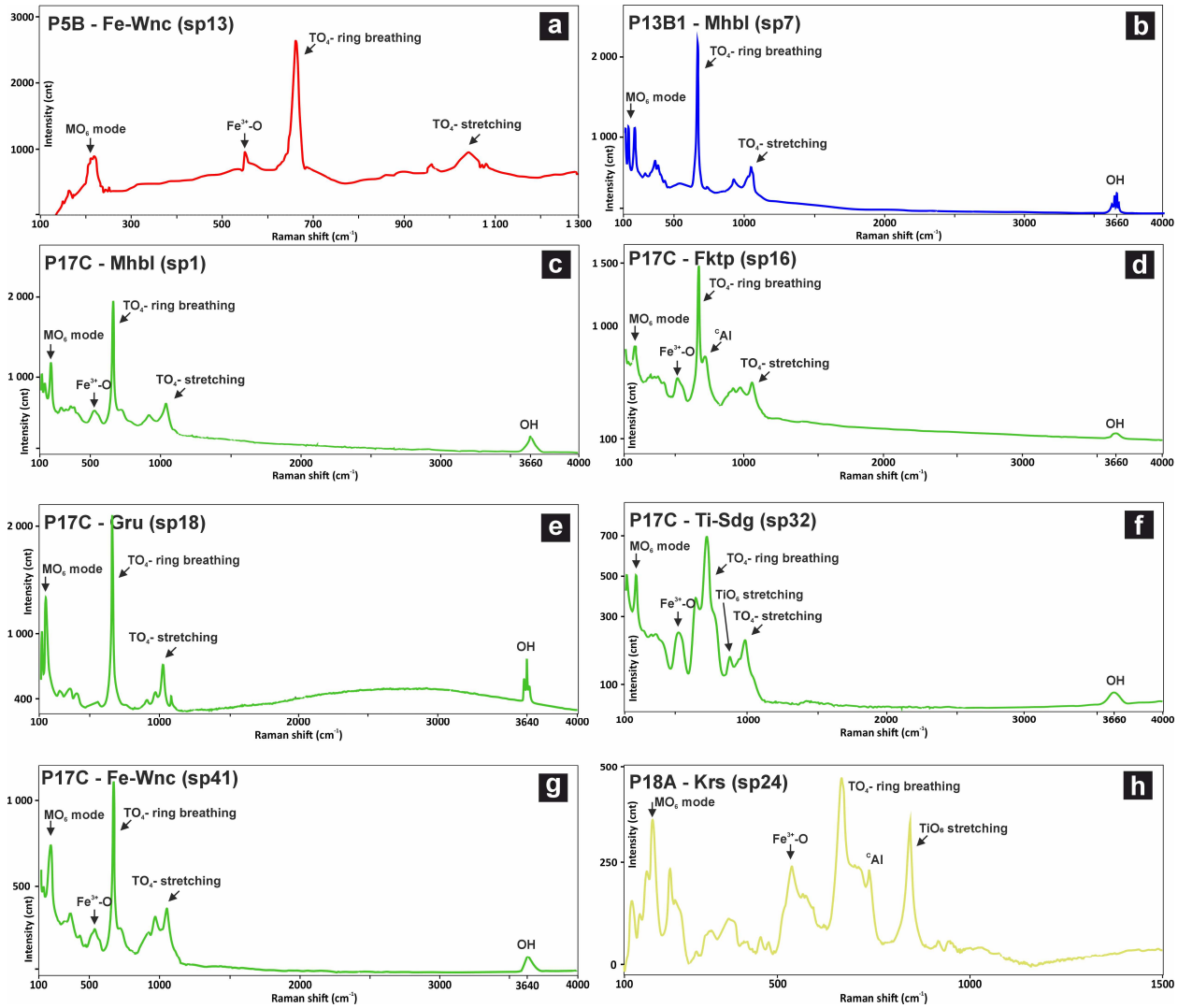


Figure 6. Micro-Raman spectra of analyzed samples from gabbro layer (**a**–**g**) and troctolite (**h**) in dunite: (**a**) Raman spectra of Amp (Fe-Wnc) in plagiogranite (P5B); (**b**) Raman spectra of Amp2 (Mhbl) in Cpx-Pl-Amp-Ilm gabbro (P13B1); (**c**) Raman spectra of Amp2 (Mhbl) in Cpx-Pl-Amp-Ilm dolerite (P17C); (**d**) Raman spectra of Amp3 (Fktp) in Cpx-Pl-Amp-Ilm dolerite (P17C); (**e**) Raman spectra of Amp4 (Gru) in Cpx-Pl-Amp-Ilm dolerite (P17C); (**f**) Raman spectra of Ti-Sdg inclusion in Amp1 from Cpx-Pl-Amp-Ilm dolerite (P17C); (**g**) Raman spectra of Amp3 (Fe-Wnc) in Cpx-Pl-Amp-Ilm dolerite (P17C); (**h**) Raman spectra of Amp (Krs) in troctolite (P18A). The place of measurements is shown by the red circle in Figure 4a–f. Amphibole types according to Tables 2–4. All the spectra were used in their raw form, not corrected to baseline.

4.4.1. Magmatic Amphiboles

The magmatic Amp1 from gabbros (P10C and P13B1) and dolerites (P16 and P17C) provides a crystallization T interval of 865 to 777 °C (avg. 801 °C) and P 0.17 to 0.10 GPa (avg. 0.13 GPa). The late magmatic Amp2 of these rocks shows a crystallization T between 837 and 661 °C (avg. 747 °C) at P between 0.31 and 0.08 GPa (avg. 0.17 GPa).

The magmatic Amp1 in dolerite dyke P9 in serpentinized peridotite shows T from 945 to 922 °C (avg. 931 °C) at 0.40–0.26 GPa (avg. 0.34 GPa), while basalt dyke P10D in the gabbro layer gabbro (P10A–C) indicates a P–T interval of 906–797 °C (avg. 852 °C) at 0.52–0.18 GPa (avg. 0.29 GPa). The leucogabbro dyke P13B2 in gabbro (P13B1) P–T is between 1094 and 1025 °C (avg. 1059 °C) at 0.33–0.28 GPa (avg. 0.30 GPa).

Table 5. Table of P–T conditions calculated from the genetically different amphibole groups. Amphibole types according to Tables 3 and S1.

Amphibole Type	**Magmatic Amphibole**				**Inclusion in Amp1**		**Amphibole from Ultramafic Rocks and Alteration Zones**				**Metamorphic Amphibole**	
Rock Type	**Gabbro, Dolerite**				**Dolerite**		**Harzburgite, Dunite, Troctolite**		**Dolerite, Leucogabbro**		**Metamorphic Sole Amphibolite**	
Amphibole gen.	*Amp1*		*Amp2*		*Amp inclusion*		*Amp in mantle rocks*		*Amp5*		*Amp6*	
Min/Max	Max	Min	Max	Min	Max	Min	Max	Min	Max	Min	Max	Min
T (°C)	1094	732	837	661	1022	1022	1000	780	398	301	664	723
P (GPa)	0.52	0.10	0.31	0.08	0.95	0.95	0.79	0.30	0.04	0.01	0.45	0.46
Avg. T (°C)	863		747		1022		853		349		694	
Avg. P (GPa)	0.23		0.17		0.95		0.64		0.03		0.46	

4.4.2. Amphiboles from Ultramafic Rocks and Alteration Zones

Amphibole5 from dolerite dyke P9 in serpentinized peridotite provides a T interval of 347–301 °C (avg. 324 °C) at 0.04–0.01 GPa (avg. 0.02 GPa). Amphibole5 in leucogabbro dyke P13B2 in gabbro (P13B1) provides 398 °C at 0.03 GPa.

Rare Amp in harzburgite P21 shows a P–T interval of 1000–815 °C (avg. 868 °C) at 0.60–0.30 GPa (avg. 0.39 GPa).

Rare Amp in dunite P18D and troctolite P18A in this dunite provides 908–780 °C (avg. 841 °C) at 0.79–0.42 GPa (avg. 0.61 GPa).

4.4.3. Metamorphic Amphiboles

Metamorphic Amp from amphibolite (P10F; Table S1) provides T and P of 723–664 °C (avg. 694 °C) at 0.46 GPa.

5. Discussion

5.1. Mineral Composition of Amphibole Generations and Petrogenetic Significance

Amphibole is an important constituent of the mafic, metamorphic, and occasionally ultramafic rocks of the Ozren ophiolite complex. The investigated amphiboles have a diverse mineralogical composition (Figure 5a–d; Tables 2–4 and S1). Using the nomenclature of the amphibole supergroup by [30], we defined the members of the calcium amphiboles (Mhbl, Prg, Hst, Sdg to Ti-Sdg, and Tr; Figure 5a), monoclinic magnesium–iron–manganese amphiboles (Gru; Figure 5b), sodium–calcium amphiboles (Fe-Wnc to Fwnc Ktp to Fktp; Figure 5c), and oxo amphiboles (Krs and Fkrs; Figure 5d).

Magmatic Amp1 (Mhbl to Prg) has been identified in nearly all the gabbroic rocks and dolerites. A specific instance is the brown Amp1 in a dolerite dyke (P9), represented by Prg or Hst (Figure 5a). Additionally, Sdg or Ti-Sdg (Figures 4e and 5a) tiny inclusions occur in a dolerite (P17C) Amp1. Prismatic and needle-like late magmatic Amp2 (Mhbl) is present at the rim of magmatic Amp1 in gabbros and dolerites (Figures 4b–e and 5a). Amphibole2 generation formed after the crystallization of Amp1, and these transitional textures from coarse-grained Amp1 to medium-grained prismatic up to needle-like Amp2 aggregates may suggest accelerated cooling following the gabbroic melt intrusion into and onto cooler peridotite.

Amphibole3 and Amp4 are relatively rare, occurring either as individual grains or in the form of zonal grains. They have hypidiomorphic to idiomorphic habitus and grow into Amp1 and Am2 aggregates (Figure 4c–e) in a dolerite (P17C) from the gabbro–dolerite layer. Dark in BSE images Amp3 (Fwnc and Fe-Wnc to Ktp and Fktp) is in the core, whereas pale Amp4 (Gru) is on the rim of the grains in dolerite (Figures 4d,e and 5b).

The generation of Na-(Ti)-rich Amp (Fwnc and Fe-Wnc) with Bt is primary magmatic in plagiogranites (P5B) but as the post-magmatic Amp3–4 in dolerites. The Amp generation of Krs to Fkrs and Phl replaces the Spl of the troctolites (Figure 4f) within the host dunite layers in peridotite. We reported troctolitization of dunite layers in peridotite by percolating basaltic melts, which crystallized Cpx and Pl in the interstitials of Ol and Spl [8]. This situation suggests that basaltic and plagiogranitic melts might have caused the formation

of the Amp3 and 4 generations in the gabbro layer and similar Amp types also in the underlying, often Pl-bearing peridotites and dunites. In addition, plagiogranite (Figure 2) with a specific magmatic Amp (Wnc; Figure 5) occurs as an individual body in direct contact with peridotite, outside of the gabbro layer remnants, the latter moreover containing a different magmatic Amp1 (Mhbl or Prg). Such a situation suggests two different melt sources for the gabbro layer and plagiogranite. The Amp3, 4 types likely formed by an interaction of hydrous melt with peridotite, dunite, troctolite, and gabbro (e.g., [35]). The water-poor 'dry' melt percolation can be related to the Cpx-Pl gabbro dyke formation, most likely in a subridge setting, whereas the 'hydrated' melt percolation produced the Cpx-Pl-Amp gabbro–dolerite dykes and plagiogranites. The latter dyke group may have been influenced by the formation of arc-type melts and fluids, the source of which can be implied from the subduction-related amphibolitic sole (Figure 2a,b).

Amphibole1–4 generations and Cpx in mafic rocks are partly or totally replaced by the low-Al Amp5 generation represented by Tr and Act (Figure 5) and are broadly characteristic of the ocean floor metamorphic alterations (e.g., [36,37]).

Amphibole6 generation (Mhbl to Prg) of metamorphic origin occurs in amphibolites from the ophiolitic thrust sheet hanging walls detected in surface outcrops (P12A) or in borehole core samples (P10F; Figures 2 and 5). The sheared domains contain relics of porphyroclastic Mhbl and Prg within dynamically recrystallized Mhbl and Prg aggregates and the newly formed Tr–Act–Ep–Zo–Czo–Chl–Phg–Ab aggregates. This Amp-type occurs in amphibolitized eclogites of the metamorphic sole in the neighboring Krivaja-Konjuh ophiolite massif [21].

Amphibole (Mhbl) was exceptionally found in a harzburgite sample (P21), where it occurs in parallel-oriented Cpx-Amp exsolution lamellae within the Opx porphyroclasts (Figures 4g and 5). This Cpx and Amp suggest the partial breakdown of Opx into the exsolution phases (e.g., [38,39]).

The Amp-rich gabbro layer, plagiogranite intrusion, gabbro–dolerite and basaltic dykes, and Amp-poor ultramafic rocks (Pl harzburgites, dunites, and troctolites) may have been influenced by arc-type magmas, as proposed in many publications (e.g., [4–7]). Moreover, transitions from a mid-ocean ridge (MOR) to a supra-subduction zone (SSZ) or back-arc basin (BAB)-type ophiolites are characteristic in the Jurassic Neotethys of the western Vardar ophiolite belt (e.g., [40] and references therein).

5.2. Relationship of Chemical Composition and Micro-Raman Spectroscopy Data

All the studied amphiboles show typical Raman spectra of the amphibole group minerals (e.g., [41–43]) and have been compared against the RRUF database [44]. The samples share a distinct band at around 150 cm^{-1}, related to MO_6 mode (Figure 6a–h) [41,45], representing the presence of ^{C}Mg in the structure [43]. The most distinctly visible band is on the Krs spectra (Figure 6h), where the ^{C}Mg content reaches up to 3.2 *apfu* (Table 4). Enhancement of Raman scattering near 530 cm^{-1} to 570 cm^{-1} (Fe^{3+}–O vibration mode) detects the presence of $^{C}Fe^{3+}$. This is most prominent regarding Fe-Wnc (Figure 6a,g) and Krs samples (Figure 6h) but also visible on Fktp (Figure 6d) and Ti-Sdg (Figure 6f). On the other hand, this band is subtle on Gru (Figure 6e) and Mhbl (Figure 6b) spectra, where we have no $^{C}Fe^{3+}$ present (Table 4). All the amphibole spectra (Figure 6a–g) show the strongest peak at 670 cm^{-1}, related to the TO_4 ring-breathing mode (and the presence of ^{T}Al in amphiboles [43]. Ferri-katophorite (Figure 6d) and Krs (Figure 6h) also show a small peak at 680 cm^{-1}. This has been previously assigned as ^{T}Al–O–Si vibrations as related to ^{T}Al [46]. However, the authors in [43] assign this band to an amount of ^{C}Al. The peak is not very distinct in our samples, probably because the amount of ^{C}Al does not reach the >0.7 *apfu* (Table 4) described by the authors. A peak at 750 cm^{-1} to 800 cm^{-1} related to TiO_6 stretching mode [46] appears on the Raman spectra of Ti-Sdg (Figure 6f) and Krs (Figure 6h), which should indicate the presence of more than 0.3 *apfu* of ^{C}Ti (Table 4), as described by [43]. Other amphiboles from our study contain mostly negligible values of ^{C}Ti (Table 4), and the peak is not visible on any other spectra. A Raman peak at around 1040 cm^{-1}

arising from the TO_4 stretching indicating $^{C}Fe^{2+}$ in the structure [43] of amphiboles is clearly visible on the Raman spectra of all the samples except Krs (Figure 6a–h), with no Fe^{2+} in the octahedral position (Table 4).

Almost all the spectra show an OH- stretching band at 3660 cm^{-1} except Gru and Fe-Wnc (sample P17C; Figure 6e,g), which exhibit a non-distinct shift to 3640 cm^{-1}. This may be due to a crystal orientation of Amp grains or caused by compositional changes at M1 and M3 sites of Amp due to a relative amount of Mg/Fe^{2+} [43] since both Gru and Fe-Wnc contain a higher amount of Fe^{2+} (>2.5 *apfu*; Table 4).

5.3. Amphibole Geothermobarometry Estimates

The Amp geothermobarometry constrains the variable P–T conditions of the Amp types and generations. Moreover, the compositional differences, especially significantly varying Ti and Al content, in one Amp generation influenced the estimated temperature and pressure intervals (Table 5 and Table S1).

Magmatic Amp1 to Amp2 generations provided average crystallization temperatures of 863 and 747 °C, respectively, in the gabbros and dolerites of the gabbro layer at relatively lower average pressures of 0.23–0.17 GPa, implying an oceanic lower crust level of about 5–7 km. However, single-Cpx thermobarometry [47] from gabbro–dolerite (P17C) and dolerite dyke (P9) constrained an earlier magmatic crystallization of Cpx at 1150 and 1100 °C and 0.37–0.18 GPa at the estimated depth of 13–5 km [8].

An exceptional Amp type with increased Al and Ti contents (Sdg to Ti-Sdg) was determined from a dolerite (P17C) of the gabbro–dolerite layer. This Amp provided the highest temperature (1022 °C) and pressure (0.95 GPa) of crystallization. However, these grains are rare and tiny (around 20µm) inclusions in Amp1 (Figure 4e), and their origin is not clear (brought about as xenocrysts by basaltic melts from a hydrous source at a depth of ca. 30 km to the gabbro layer?).

Amphibole3 and Amp4, such as Fwnc, Fe-Wnc, Ktp, Fktp, Gru, Krs, or Fkrs, were compositionally not suitable for the available geothermobarometers. Their special chemical composition may indicate a different melt/fluid source compared to common gabbro–dolerites, which we connect with the compositionally variable percolating melts and fluids through the peridotite and the gabbro–dolerite layers (see Section 5.1).

Amphibole (Mhbl to Prg) in ultramafic rocks (harzburgite, dunite, and troctolite) provided a temperature interval of 1000–780 °C at 0.79–0.30 GPa (Table S1). These estimates are lower than those provided for Cpx from troctolite (P18A) by single-Cpx thermobarometry [47] at 1200–1100 °C at 0.45–0.15 GPa [8]. However, the Cpx from the exsolution lamellae in Opx1 from harzburgite P21 provided temperatures of 950–850 °C at maximum 1 GPa [8], which is comparable with the temperatures of 1000–815 °C at 0.60–0.30 GPa obtained from Amp geothermobarometry from this sample (Table S1). These results suggest that the Amp in P21 harzburgite indicates cooling temperatures below 1000 °C at the estimated depths of ca. 20 to 10 km, when the exsolution lamellae of Cpx and Amp have formed within the Opx1 porphyroclasts (e.g., [38,39]). The more variable and decreasing pressures imply an extension and exhumation of the mantle section of the OOC to shallower lithospheric levels, where these rocks were crosscut by numerous gabbroic–doleritic dykes. This process also explains the hydrated percolating melts/fluids as a potential source of special Na–Ti-rich Amp3 and 4 in the gabbro layer gabbros and dolerites, but a similar type of Amp also in the underlying mantle rocks, such as troctolites (~Cpx-Pl-enriched dunites) and Pl bearing peridotites [8].

The lowest temperatures of ca. 400–300 °C and pressures 0.04–0.01 GPa were estimated from the latest Amp5 generation, which replaces the Amp1 to Amp4 in a dolerite. Such conditions are consistent with the ocean-floor-type metamorphic alterations. Other authors [36] suggested 200–300 °C at maximum 0.05 GPa for gabbro rodingitization by fluids related to serpentinization of host peridotites at the ocean floor.

The higher medium-temperature and medium-pressure conditions were constrained from the metamorphic Amp of sole amphibolites. The estimates from a borehole sam-

ple (P10F) of 723–664 °C and 0.46–0.45 GPa are slightly different from 620–600 °C and 0.85–0.6 GPa estimated from a surface outcrop of amphibolites by Ti-in-Amp thermometry and Amp–Pl thermobarometry by [8], which are related to the different exhumation depths. Eclogite and amphibolite facies conditions were estimated from the metamorphic sole of the neighboring Krivaja-Konjuh Massif by [21].

6. Conclusions

1. The complex geological setting of the Ozren ophiolite complex is also confirmed by the compositionally diverse amphiboles. Here, we determined members of the monoclinic magnesium–iron–manganese amphiboles (Gru), calcium amphiboles (Mhbl, Prg, Hst, Sdg to Ti-Sdg, and Tr), sodium–calcium amphiboles (Fe-Wnc to Fwnc Ktp to Fktp), and oxo amphiboles (Krs and Fkrs).
2. The chemical composition of the studied amphiboles provided a very good correlation with the analyzed Raman spectra.
3. Electron probe micro-analysis (EPMA), micro-Raman study, and Amp geothermobarometry constrained the genetically different Amp groups and types (Table 3) in the investigated oceanic crust and mantle rocks:

Primary magmatic Amp1 (Mhbl to Prg, rarely Hst) is present in almost all the gabbroic rocks and dolerites. Tiny inclusions of Sdg or Ti-Sdg grains in Amp1 may suggest a deeper and hotter hydrated source during the formation of the gabbro–dolerite layer.

Na-(Ti)-rich Amp (Fwnc and Fe-Wnc) occurs as the primary magmatic Amp in plagiogranites.

Late magmatic prismatic and needle-like Amp2 (Mhbl) in gabbros and dolerites followed the crystallization of coarse-grained Amp1 due to cooling of emplaced gabbroic melts in the lower oceanic crust.

Amphibole3 (Fwnc, Fe-Wnc to Ktp, and Fktp) and Amp4 (Gru) in a dolerite of the gabbro–dolerite layer are most likely linked to percolating melts/fluids accompanying the emplacement of gabbroic–doleritic dykes in peridotites, dunites, and the gabbro layer.

Similarly, Ti-rich Amp (Krs to Fkrs) associated with Phl in troctolites may indicate 'hydrated' melt percolation produced by Cpx-Pl-Amp gabbro–dolerite dykes and plagiogranitic intrusions in the lower oceanic crust and the underlying mantle rocks.

Low-Al Amp5 generation (Tr and Act) partly or totally replaces Amphibole1–4 and Cpx in mafic rocks, suggesting ocean-floor-type alterations.

Metamorphic Amphibole6 (Mhbl to Prg) occurs in subduction-related sole amphibolites.

4. 'Dry' percolating melts are most likely generated in an extensional subridge setting, while 'hydrated' Amp-bearing rocks may have been influenced by arc-type magmas and fluids, implying a change from the mid-ocean ridge (MOR) to a supra-subduction zone (SSZ) setting of the Ozren ophiolite complex.

Supplementary Materials: The following supporting information can be downloaded at: https://www.mdpi.com/article/10.3390/min14030239/s1, Table S1: EPMA analyses of amphiboles used for the Amp geothermobarometry and additional Amp types.

Author Contributions: Conceptualization, S.U. and M.P.; methodology, S.U., O.N. and S.M.; software, O.N., S.M. and S.K.; validation, M.P.; formal analysis, S.U., O.N., S.M. and M.P.; investigation, S.U., E.B., M.P. and P.R.; resources, M.P., E.B., P.R., S.K. and S.M.; data curation, S.U. and O.N.; writing—original draft preparation, S.U., O.N. and M.P.; writing—review and editing, M.P. and E.B.; visualization, S.U., O.N. and S.M.; supervision, M.P. and E.B.; project administration, M.P.; funding acquisition, M.P. and S.U. All authors have read and agreed to the published version of the manuscript.

Funding: Funding from the Slovak Research and Development Agency projects (APVV-19-0065 and APVV-22-0092), VEGA agency (1/0028/24), and Comenius University grant (UK/37/2022) is greatly appreciated.

Data Availability Statement: The data presented in this study are available in Supplementary Material here.

Acknowledgments: Review reports of the three referees who contributed to the original manuscript improvement are greatly acknowledged. We appreciate very much the language correction of the submitted manuscript.

Conflicts of Interest: The authors declare no conflicts of interest.

References

1. Welch, D.M. Amphiboles. In *Encyclopedia of Geology*, 2nd ed.; Elias, S., Alderton, D., Eds.; Academic Press: Cambridge, MA, USA, 2020; pp. 297–300. ISBN 978-0081029084.
2. Dilek, Y.; Furnes, H. Ophiolite genesis and global tectonics: Geochemical and tectonic fingerprinting of ancient oceanic lithosphere. *Geol. Soc. Am. Bull.* **2011**, *123*, 387–411. [CrossRef]
3. Basch, V.; Rampone, E.; Crispini, L.; Ferrando, C.; Ildefonse, B.; Godard, M. Multi-stage Reactive Formation of Troctolites in Slow-spreading Oceanic Lithosphere (Erro–Tobbio, Italy): A Combined Field and Petrochemical Study. *J. Petrol.* **2019**, *60*, 873–906. [CrossRef]
4. Itano, K.; Morishita, T.; Nishio, I.; Guotana, J.M.; Ogusu, Y.; Ishizuka, O.; Tamura, A. Petrogenesis of amphibole-rich ultramafic rocks in the Hida metamorphic complex, Japan: Its role in arc crust differentiation. *Lithos* **2021**, *404*, 106440. [CrossRef]
5. Alonso-Perez, R.; Müntener, O.; Ulmer, P. Igneous garnet and amphibole fractionation in the roots of island arcs: Experimental constraints on andesitic liquids. *Contrib. Mineral. Petrol.* **2009**, *157*, 541–558. [CrossRef]
6. Ishimaru, S.; Arai, S.; Tamura, A.; Takeuchi, M.; Kiji, M. Subarc magmatic and hydration processes inferred from a hornblende peridotite xenolith in spessartite from Kyoto, Japan. *J. Mineral. Petrol. Sci.* **2009**, *104*, 97–104. [CrossRef]
7. Tiepolo, M.; Langone, A.; Morishita, T.; Yuhara, M. On the Recycling of Amphibole-rich Ultramafic Intrusive Rocks in the Arc Crust: Evidence from Shikanoshima Island (Kyushu, Japan). *J. Petrol.* **2012**, *53*, 1255–1285. [CrossRef]
8. Putiš, M.; Nemec, O.; Ustalić, S.; Babajić, E.; Ružička, P.; Koller, F.; Kurylo, S.; Katanić, P. Mineralogical-Petrographical Record of Melt-Rock Interaction and P–T estimates from the Ozren Massif Ophiolites (Bosnia and Herzegovina). *Minerals* **2022**, *12*, 1108. [CrossRef]
9. Colombo, F.; Rius, J.; Molins, E.; Biglia, H.; Galliski, M.Á.; Márquez-Zavalía, M.F.; Baldo, E.G.A.; Kriscautzky, A. Ferro-ferri-katophorite, a new clinoamphibole from the silicocarbonatite dykes in Sierra de Maz, La Rioja, Argentina. *Mineral. Mag.* **2023**, *87*, 324–330. [CrossRef]
10. Schmid, S.M.; Bernoulli, D.; Fügenshuh, B.; Matenco, L.; Schefer, S.; Schuster, R.; Tischler, M.; Ustaszewski, K. The Alpine–Carparthian–Dinaric orogenic system: Compilation and evolution of tectonic units. *Swiss J. Geosci.* **2008**, *101*, 139–183. [CrossRef]
11. Robertson, A.; Karamata, S.; Šarić, K. Overview of ophiolites and related units in the late Palaeozoic–early Cenozoic magmatic and tectonic development of Tethys in the northern part of the Balkan region. *Lithos* **2009**, *108*, 1–36. [CrossRef]
12. Trubelja, F.; Pamić, J. Petrologic study of mountain Ozren in the north of Bosnia. *Acta Geol.* **1965**, *IV*, 265–314.
13. Lugović, B.; Altherr, R.; Raczek, I.; Hoffmann, A.; Majer, V. Geochemistry of peridotites and mafic igneous rocks from the Central Dinaric ophiolite belt, Yugoslavia. *Contrib. Mineral. Petrol.* **1991**, *106*, 201–216. [CrossRef]
14. Pamić, J.; Tomljenović, B.; Balen, D. Geodynamic and petrogenetic evolution of Alpine ophiolites from the central and NW Dinarides: An overview. *Lithos* **2002**, *65*, 113–142. [CrossRef]
15. Karamata, S. The geological development of the Balkan Peninsula related to the approach, collision and compression of Gondwanan and Eurasian units. *Geol. Soc. Lond. Spec. Publ.* **2006**, *260*, 155–178. [CrossRef]
16. Bazylev, B.A.; Popević, A.; Karamata, S.; Kononkova, N.N.; Simakin, S.G.; Olujić, J.; Vujnović, L.; Memović, E. Mantle peridotites from the Dinaridic ophiolite belt and the Vardar zone western belt, Central Balkan. *Lithos* **2009**, *108*, 37–71. [CrossRef]
17. Ustaszewski, K.; Kounov, A.; Schmid, S.M.; Schaltegger, U.; Krenn, E.; Frank, W.; Fügenschuh, B. Evolution of the Adria-Europe plate boundary in the northern Dinarides: From continent-continent collision to back-arc extension. *Tectonics* **2010**, *29*, TC6017. [CrossRef]
18. Morishita, T.; Dilek, Y.; Shallo, M.; Tamura, A.; Arai, S. Insight into the uppermost mantle section of a maturing arc: The eastern Mirdita ophiolite, Albania. *Lithos* **2011**, *124*, 215–226. [CrossRef]
19. Faul, U.H.; Garapić, G.; Lugović, B. Subcontinental rift initiation and ocean-continent transitional setting of the Dinarides and Vardar zone: Evidence from the Krivaja–Konjuh Massif, Bosnia and Herzegovina. *Lithos* **2014**, *202*, 283–299. [CrossRef]
20. Šegvić, B.; Slovenec, D.; Schuster, R.; Babajić, E.; Badurina, L.; Lugović, B. Sm-Nd geochronology and petrologic investigation of a sub-ophiolite metamorphic sole from the Dinarides (Krivaja-Konjuh Ophiolite Complex, Bosnia and Herzegovina). *Geol. Croat.* **2020**, *73*, 119–130. [CrossRef]
21. Balen, D.; Massonne, H.J. Two contrasting P-T paths for metamorphic sole amphibolites of the Dinaride Ophiolite Zone (Krivaja-Konjuh ultramafic massif, Central Bosnia and Herzegovina) and their geodynamic implications. *Lithos* **2021**, *394*, 106184. [CrossRef]
22. Ustalić, S.; Putiš, M.; Nemec, O.; Ružička, P.; Babajić, E.; Katanić, P. Petrography of ultrabasic and basic rocks from the Ozren ophiolite complex in Bosnia and Herzegovina. In Proceedings of the 15th Emile Argand Conference on Alpine Geological Studies: Abstract Book and Fieldtrip Guide, Ljubljana, Slovenia, 12–14 September 2022; Volume 66. [CrossRef]

23. Ustalić, S.; Putiš, M.; Babajić, E.; Nemec, O.; Ružička, P. Lithological cross-section and mineralogical-petrographical characterization of the Ozren and Borja-Mahnjača ophiolite complexes in Bosnia and Herzegovina. In Proceedings of the Scientific Conference of the Slovak Geological Society, Newsletter of the SGS Mente et Malleo 2/2022, Abstracts, Bratislava, Slovakia, 13 January 2023; pp. 47–48.
24. Soták, J.; Ustalić, S.; Putiš, M.; Babajić, E.; Ružička, P. New radiolarian data from the Ozren ophiolite complex in Bosnia and Herzegovina. In Proceedings of the III Congress of Geologists of Bosnia and Herzegovina with International Participation, Neum, Bosnia and Herzegovina, 21–23 September 2023; pp. 38–41.
25. Ustalić, S.; Soták, J.; Putiš, M.; Babajić, E.; Ružička, P. Comparative study of radiolarians from the Ozren and Borja-Mahnjača Dinaridic ophiolitic massifs in Bosnia and Herzegovina. *Sci. Conf. Slovak Geol. Soc. Newsl. SGS Mente Et Malleo* **2023**, *2023*, 29.
26. Sunarić-Pamić, O.; Pamić, J.; Kapelar, I.; Olujić, J.; Zec, F. The Basic Geological Map of the Former SFR Yugoslavia 1:100 000, Geological Sheet Zavidovići. Repub. Geol. Surv. Geol. Surv. Sarajevo Bosnia Herzeg. 1971.
27. Laušević, M.; Jovanović, Č. The Basic Geological Map of the Former SFR Yugoslavia 1:100,000, Geological Sheet Doboj. Repub. Geol. Surv. Geoinženjering Inst. Sarajevo Sarajevo Bosnia Herzeg. 1982.
28. Locock, A.J. An Excel spreadsheet to classify chemical analyses of amphiboles following the IMA 2012 recommendations. *Comput. Geosci.* **2014**, *62*, 1–11. [CrossRef]
29. Leake, B.E. Nomenclature of amphiboles. *Mineral. Mag.* **1978**, *42*, 533–563. [CrossRef]
30. Hawthorne, F.; Oberti, R.; Harlow, G.; Maresch, W.; Martin, R.F.; Schumacher, J.; Welch, M. IMA report: Nomenclature of the amphibole supergroup. *Am. Mineral.* **2012**, *97*, 2031–2048. [CrossRef]
31. Oberti, R.; Boiocchi, M.; Hawthorne, F.; Cámara, F.; Ciriotti, M.; Berge, S. Ti-rich fluoro-richterite from Kariasen (Norway): The oxo-component and the use of Ti^{4+} as a proxy. *Can. Mineral.* **2015**, *53*, 285–294. [CrossRef]
32. Ridolfi, F. Amp-TB2: An Updated Model for Calcic Amphibole Thermobarometry. *Minerals* **2021**, *11*, 324. [CrossRef]
33. Ernst, W.G.; Liu, J. Experimental phase-equilibrium study of Al- and Ti-contents of calcic amphibole in MORB; a semiquantitative thermobarometer. *Am. Mineral.* **1998**, *83*, 952–969. [CrossRef]
34. Warr, L.N. IMA–CNMNC approved mineral symbols. *Mineral. Mag.* **2021**, *85*, 291–320. [CrossRef]
35. Bonadiman, C.; Nazzareni, S.; Coltorti, M.; Comodi, P.; Giuli, G.; Faccini, B. Crystal chemistry of amphiboles: Implications for oxygen fugacity and water activity in lithospheric mantle beneath Victoria land, Antarctica. *Contrib. Mineral. Petrol.* **2014**, *167*, 984. [CrossRef]
36. Bach, W.; Klein, F. The petrology of seafloor rodingites: Insights from geochemical reaction path modeling. *Lithos* **2009**, *112*, 103–117. [CrossRef]
37. Bucher, K.; Grapes, R. *Petrogenesis of Metamorphic Rocks*; Springer: Berlin/Heidelberg, Germany, 2011; pp. 1–428. [CrossRef]
38. Saveliev, D.E.; Puchkov, V.N.; Sergeev, S.N.; Musabirov, I.I. Deformation-induced decomposition of enstatite in mantle peridotite and its role in partial melting and chromite ore formation. *Dokl. Earth Sci.* **2017**, *476*, 1058–1061. [CrossRef]
39. Putiš, M.; Li, X.-H.; Yang, Y.-H.; Li, Q.-L.; Nemec, O.; Ling, X.-X.; Koller, F.; Balen, D. Permian pyroxenite dikes in harzburgite with signatures of the mantle, subduction channel and accretionary wedge evolution (Austroalpine Unit, Eastern Alps). *Lithos* **2018**, *314*, 165–186. [CrossRef]
40. Maffione, M.; van Hinsbergen, D.J.J. Reconstructing Plate Boundaries in the Jurassic Neo-Tethys from the East and West Vardar Ophiolites (Greece and Serbia). *Tectonics* **2018**, *37*, 858–887. [CrossRef]
41. Apopei, A.I.; Buzgar, N. The Raman study of Amphiboles. *Anal. Şt. Univ. Al. I. Cuza Iaşi–Geologie. Tomul LVI* **2010**, *1*, 57–83.
42. Andò, S.; Garzanti, E. Raman spectroscopy in heavy-mineral studies. *Geol. Soc. Lond. Spec. Publ.* **2013**, *386*, 395–412. [CrossRef]
43. Waeselmann, N.; Schlüter, J.; Malcherek, T.; Della Ventura, G.; Oberti, R.; Mihailova, B. Nondestructive determination of the amphibole crystal-chemical formulae by Raman spectroscopy: One step closer. *J. Raman Spectrosc.* **2019**, *51*, 1530–1548. [CrossRef]
44. Lafuente, B.; Downs, R.T.; Yang, H.; Stone, N. The power of databases: The RRUFF project. In *Highlights in Mineralogical Crystallography*; Armbruster, T., Danisi, R., Eds.; Walter de Gruyter GmbH: Berlin, Germany, 2016; pp. 1–29. [CrossRef]
45. Susta, U.; Della Ventura, G.; Hawthorne, F.C.; Abdu, Y.A.; Day, M.C.; Mihailova, B.; Oberti, R. The crystal-chemistry of riebeckite, ideally $Na_2Fe^{2+}{}_3Fe^{3+}{}_2Si_8O_{22}(OH)_2$: A multitechnique study. *Mineral. Mag.* **2018**, *82*, 837–852. [CrossRef]
46. Apopei, A.I.; Buzgar, N.; Buzatu, A. Raman and infrared spectroscopy of kaersutite and certain common amphiboles. *Analele Stiintifice ale Universitatii Al. I. Cuza din Iasi. Seria Geologie.* **2011**, *57*, 35–58.
47. Wang, X.; Hou, T.; Wang, M.; Zhang, C.; Zhang, Z.; Pan, R.; Marxer, F.; Zhang, H. A new clinopyroxene thermobarometer for mafic to intermediate magmatic systems. *Eur. J. Mineral.* **2021**, *33*, 621–637. [CrossRef]

Disclaimer/Publisher's Note: The statements, opinions and data contained in all publications are solely those of the individual author(s) and contributor(s) and not of MDPI and/or the editor(s). MDPI and/or the editor(s) disclaim responsibility for any injury to people or property resulting from any ideas, methods, instructions or products referred to in the content.